Research article

Potential of lncRNAs to regulate cuproptosis in hepatocellular carcinoma: Establishment and validation of a novel risk model

Jing He [a,b,c,d,e,1], Weiqi Li [a,b,c,d,e,1], Weijun Zhao [a,b,c,d,e,1], Hao Shen [a,b,c,d,e], Yushun Chang [a,b,c,d,e], Boqiang Liu [a,b,c,d,e], Qiang He [f], Hong Yu [a,b,c,d,e], Yifan Wang [a,b,c,d,e,***], Liang Shi [a,b,c,d,e,**], Xiujun Cai [a,b,c,d,e,*]

[a] Zhejiang Provincial Key Laboratory of Laparoscopic Technology, Sir Run Run Shaw Hospital, Zhejiang University, Hangzhou, 310016, China
[b] Department of General Surgery, Sir Run Run Shaw Hospital, School of Medicine, Zhejiang University, Hangzhou, 310016, China
[c] Zhejiang Minimal Invasive Diagnosis and Treatment Technology Research Center of Severe Hepatobiliary Disease, Zhejiang University, Hangzhou, 310016, China
[d] Zhejiang Research and Development Engineering Laboratory of Minimally Invasive Technology and Equipment, Zhejiang University, Hangzhou, 310016, China
[e] Zhejiang University Cancer Center, Zhejiang University, Hangzhou, 310016, China
[f] Department of Hepatobiliary Surgery, Linyi People's Hospital, Linyi, Shandong, China

ARTICLE INFO

ABSTRACT

Cuproptosis, a distinct form of programmed cell death, is an emerging field in oncology with promising implications. This novel mode of cell death has the potential to become a regulatory target for tumor therapy, thus expanding the currently limited treatment options available for patients with cancer. Our research team focused on investigating the role of functional long non-coding RNA (lncRNAs) in hepatocellular carcinoma (HCC). We were particularly intrigued by the potential implications of HCC-lncRNAs on cuproptosis. Through a comprehensive analysis, we identified three cuproptosis-related lncRNAs (CRLs): AC018690.1, AL050341.2, and LINC02038. These lncRNAs were found to influence the sensitivity of HCC to cuproptosis. Based on our results, we constructed a risk model represented by the equation: risk score = 0.82 * *AC018690.1* + 0.65 * *AL050341.2* + 0.61 * *LINC02038*. Notably, significant disparities were observed in clinical features, such as the response rate to immunotherapy and targeted therapy, as well as in cellular characteristics, including the composition of the tumor immune microenvironment (TIME), when comparing the high- and low-risk groups. Most importantly, knockdown of these CRLs was confirmed to significantly weaken the resistance to cuproptosis in HCC. This effect resulted from the accelerated accumulation of lipoacylated-DLAT and lipoacylated-DLST. In summary, we identified three CRLs in HCC and established a novel risk model with potential clinical applications. Additionally, we proposed a potential therapeutic method consisting of sorafenib-copper ionophores-immunotherapy.

* Corresponding author. Department of General Surgery, Sir Run-Run Shaw Hospital, Zhejiang University, China.
** Corresponding author. Department of General Surgery, Sir Run-Run Shaw Hospital, Zhejiang University, China.
*** Corresponding author. Department of General Surgery, Sir Run-Run Shaw Hospital, Zhejiang University, China.
E-mail addresses: anwyf@zju.edu.cn (Y. Wang), Liang_Shi@zju.edu.cn (L. Shi), srrsh_cxj@zju.edu.cn (X. Cai).
[1] These authors contributed equally to this work.

1. Introduction

Hepatocellular carcinoma (HCC) stands as a prevalent form of primary liver cancer and is globally the second leading cause of cancer-related deaths [1,2]. Unfortunately, the incidence of HCC has surged unpredictably on a global scale. HBV emerges as a major risk factor for HCC [3], and an additional contributing factor is the obesity epidemic, leading to the development of nonalcoholic fatty liver disease and nonalcoholic steatohepatitis [4,5]. The most effective treatment, surgery, confers benefits primarily to a limited subset of patients in the early stages [6]. Unfortunately, it is often the case that patients are diagnosed with cancer when it has already reached an advanced stage. In such instances, tumors often display resistance to traditional chemotherapy or radiotherapy, curtailing the effectiveness of these treatments [7]. The intricate biology of HCC poses a substantial obstacle to the advancement of more refined and targeted therapeutic approaches. Therefore, it is imperative to accurately identify specific targets for HCC and develop therapeutic strategies that prove effective.

Copper serves as an indispensable catalytic and structural cofactor, instigating alterations in protein structure, catalytic activity, and protein-protein interactions that drive crucial biochemical processes vital to life [8,9]. The regulation of copper homeostasis is meticulous, maintaining copper levels at exceptionally low levels under normal conditions [10]. Anomalies in copper metabolism are linked to conditions such as anemia, metabolic and neurological diseases, and cancer [11,12]. Existing data suggest an excessive accumulation of copper in HCC [13]. Notably, copper has been identified as a key player in expediting the proliferation, invasive behavior, and metastatic potential of malignant cells [14]. In a recent notable study by Tsvetkov et al., copper-dependent death was proposed, involving the direct binding of copper to fatty acylated components of the tricarboxylic acid (TCA) cycle, a phenomenon termed cuproptosis [15]. Investigating the molecules that regulate this distinctive form of cellular death has the potential to deepen our understanding and uncover possible applications in clinical interventions for HCC.

Long non-coding RNAs (lncRNAs) represent a functionally diverse group of non-coding RNAs (ncRNAs) abundant in the human transcriptome. However, the mechanisms underlying the functions of most lncRNAs in cells remain poorly understood [16]. It is increasingly evident that a large proportion of lncRNAs play crucial roles in regulating normal cellular physiology and are implicated in various diseases, including cancer [17,18]. While some studies have utilized bioinformatics techniques to identify cuproptosis-related lncRNAs (CRLs) in HCC, the involvement of CRLs in the intricate process of cuproptosis, particularly in cancer, remains largely unknown. The regulatory mechanisms governing this phenomenon are yet to be clarified.

In this study, we aimed to identify essential CRLs and explore their significance in the progression and development of HCC. We developed a cuproptosis-related risk model through a comprehensive analysis method that integrated both coding and non-coding RNA expression data, along with survival data from patients with HCC. Analyzing the biological activity of CRLs, we compared the features of the risk groups. In vitro experiments were conducted to validate the role of these lncRNAs in regulating cuproptosis. Our study underscores the significance of CRLs in HCC, providing a foundational understanding for the potential clinical application of copper ionophores.

2. Materials and methods

2.1. Datasets

We obtained FPKM-normalized RNA-seq data from 374 tumor samples, along with corresponding clinical data, from The Cancer Genome Atlas (TCGA) database (https://portal.gdc.cancer.gov/projects/TCGA-LIHC). Patients with incomplete clinical data were excluded. Additionally, we acquired the GSE115018 dataset, which includes 12 HCC tissues and 12 paracancerous normal tissues, from the Gene Expression Omnibus (GEO) database (https://www.ncbi.nlm.nih.gov/geo/). This dataset served as the validation dataset.

2.2. Patient samples

For validation purposes, six patients with HCC were included in this study. This group comprised three high-invasive (HI) HCC tissues, characterized by tumor diameters smaller than 3 cm and diagnosed with postsurgical metastasis or recurrence, and three low-invasive (LI) HCC tissues, characterized by tumor diameters larger than 3 cm and postsurgical metastasis or recurrence negativity. All clinical samples were collected from Sir Run Run Shaw Hospital in Hangzhou, China. The study adhered to the principles of the Declaration of Helsinki and received approval from the institutional review board of Sir Run Run Shaw Hospital. Written informed consent was obtained from all patients before surgery for the use of their tissues in scientific research.

2.3. Next generation sequencing

Total RNA was extracted using the TRIzol reagent (Invitrogen) following the manufacturer's instructions. The concentration and quality of total RNA were assessed using a Nanodrop spectrophotometer and verified by gel electrophoresis. Subsequently, the total RNA samples were sent to TSINGKE Biological Technology Co., Ltd. for library construction, sequencing, and analysis.

2.4. Differential expression analysis of lncRNAs

For the identification of lncRNAs exhibiting significant differential expression between HCC and normal liver tissues (TCGA dataset), we utilized the R package "limma (version: 3.58.1) ". The screening criteria applied were $|\log2 (\text{Fold Change})| > 1$ and

adjusted p-value <0.01. The Benjamini–Hochberg (BH) method was employed for p-value correction.

3. Identification of CRLs in HCC

Cuproptosis-related genes (CRGs) were obtained from a study conducted by Tsvetkov et al. [15]. Subsequently, we investigated lncRNAs exhibiting correlation with CRGs based on FPKM values, utilizing Pearson's correlation analysis with a threshold of R > 0.3 and a p-value <0.0001 as the statistical criteria.

3.1. Construction of a cuproptosis-related risk model

To address the scarcity of HCC public datasets containing ncRNAs, mRNA expression profiles, and clinical data, we utilized the "createDataPartition" function from the R package "caret (version: 6.0–94)". This function randomly divided patients with HCC (TCGA datasets) into training and test groups in a 1:1 ratio. A statistical analysis (chi-square test, p-value >0.05) confirmed no significant differences in clinical information between the two groups (Supplementary Table 1). Survival analysis, incorporating the overlap between CRLs and differentially expressed lncRNAs, was conducted using the R package "survival (version: 3.5–7)". Initially, CRLs associated with patient prognosis were identified through univariate Cox analysis (p-value <0.05). To mitigate multicollinearity, we employed LASSO regression analysis, cross-validated ten times for robustness. Subsequently, multivariate Cox analysis assessed the independent impact of screening CRLs on patient prognosis and facilitated the development of a risk model. The computational formula for the cuproptosis-related risk score is given by: risk score = Coef_i *lncRNA1* $\times$ *lncRNA1* expression + Coef_i *lncRNA2* $\times$ *lncRNA2* expression + $\cdots\cdots$ +Coef_i *lncRNAn* $\times$ *lncRNAn* expression, where n represents the number of CRLs, and Coefi denotes the coefficient of the corresponding lncRNA. This formula calculates risk scores for each sample. Subsequently, the TCGA dataset and additional datasets (GSE115018 and clinical HCC samples) were partitioned into high- and low-risk groups based on the median risk score.

3.2. Principal component analysis (PCA)

To evaluate the effectiveness of the constructed risk model in differentiating between patients in high- and low-risk groups, we performed PCA using the R package "limma (version: 3.58.1)" on the TCGA dataset. This analysis aimed to assess the accuracy of the model and its ability to capture meaningful distinctions based on the expression of CRLs.

3.3. Validation of cuproptosis-related risk model based on CRLs

We conducted risk curve and survival analyses on the cuproptosis-related risk model for the entire sample, as well as the training and test groups. Kaplan–Meier survival curves were generated using the R packages "survival (version: 3.5–7)" and "survminer (version: 0.4.9)". The aim was to assess the relationship between overall survival (OS) and disease-free survival (DFS) in connection with the risk scores of patients categorized into high- and low-risk groups. Furthermore, we utilized the Wilcoxon rank-sum test to compare risk scores in the validation datasets (GSE115038 and clinical HCC samples).

3.4. Optimization of cuproptosis-related risk model

To enhance the cuproptosis-related risk model, we analyzed clinical indicators of patients with HCC (Supplementary Table 2) using the R package "survival (version: 3.5–7)". Factors influencing survival (with a p-value <0.05) were incorporated into the model. Subsequently, we employed the R packages "survival (version: 3.5–7)" and "rms (version: 6.3–0)" to construct a nomogram for predicting 1-, 3-, and 5-year survival in patients with HCC. To assess the predictive accuracy of the optimized risk model, a calibration curve was utilized.

3.5. Analysis of tumor immune microenvironment (TIME)

We applied the "ssGSEA" algorithm, implemented in the R package "GSVA (version: 1.50.0)" to assess the abundance of 23 distinct immune cell types infiltrating each sample [19]. Pearson's correlation analysis was employed to evaluate the relationship between the risk score and the abundance of immune cells. Tumor Immune Dysfunction and Exclusion (TIDE), an indicator predicting the response of a patient to immunotherapy [20,21], underwent assessment through Analysis of Variance (ANOVA) to compare immune characteristics between risk groups.

3.6. Comparison of tumor mutational burden among risk groups

Using the R package "maftools (version: 2.18.0)", we extracted the Mutation Annotation Format (MAF) from the TCGA database. This study aimed to examine the mutational landscape of patients with HCC in different cuproptosis-related risk groups.

3.7. Drug susceptibility analysis

To investigate the therapeutic effects of drugs in the two groups, we calculated the semi-inhibitory concentration (IC50) values of drugs using the R package "pRRophetic".

3.8. Function enrichment analysis

For Gene Ontology (GO) and Kyoto Encyclopedia of Genes and Genomes (KEGG) enrichment analysis, we employed the R packages "clusterProfiler (version: 4.10.0)" and "org.Hs.eg.db (version: 3.18.0)". The BH method was applied for p-value correction, with a threshold set at p-value <0.05.

3.9. Reagents

Detail of these reagents were included in Supplementary Materials.

3.10. Cell culture

Huh7 cells were cultured in MEM (Invitrogen, Grand Island, NY, USA) supplemented with 10 % fetal bovine serum (FBS) and 1 % glutamine, while HCCLM3 cells were maintained in DMEM (Invitrogen, Grand Island, NY) with 10 % FBS, and 1 % glutamine. HCCLM3 was maintained in DMEM (Invitrogen, Grand Island, NY) with 10 % FBS and 1 % glutamine. All cells were cultured at 37 °C and 5 % CO2. Rigorous quality control measures were implemented, including mycoplasma testing through a polymerase chain reaction (PCR)-based method and DAPI staining to confirm the absence of contamination. Detailed information on cell line sources is provided in the Supplementary Materials.

3.11. Copper ionophores-induced cell death assay

For siRNA transfection, Lipofectamine 3000 (Invitrogen, Carlsbad, CA, USA) was utilized following the manufacturer's instructions. Supplementary Materials contain the siRNA sequences used. After 48 h of transfection, copper ionophores (elesclomol) and CuCl2 were introduced at the specified concentrations, with a medium change after 2 h of shock. Subsequently, after 20 h, the medium was collected, adherent cells were digested, and the cell suspension was centrifuged at 2000 rpm for 15 min. CFSE (Invitrogen) was diluted in PBS (1:3000), and the cells were resuspended, followed by an incubation at room temperature in the dark for 15 min. Flow cytometry (BD LSRFortessa) was employed for detection, utilizing excitation light at 488 nm.

3.12. RNA extraction and quantitative real-time PCR

RNA extraction was performed using an RNA-Quick Purification Kit (ES Science). Subsequently, the extracted RNA underwent reverse transcription using an Eco M-MLV RT Premix Kit (AG11706; Accurate Biology). The expression of target genes was normalized to that of the endogenous control gene glyceraldehyde 3-phosphate dehydrogenase (GAPDH). RT-qPCR was conducted on Quant-Studio 1 (Applied Biosystems, Thermo Fisher Scientific, USA) using a SYBR Green Premix Pro Tag HS qPCR kit (AG11701, Accurate Biology). The $2^{-\Delta\Delta CT}$ method was employed to calculate lncRNA expression levels. Primer sequences used for RT-qPCR are provided in the Supplementary Materials.

*3.13. Cell lysis and immunoblotting (IB)*

For cell lysis, cells were homogenized in RIPA or IP lysis buffer supplemented with a Protease Inhibitor Cocktail, Phosphatase Inhibitor Cocktail, Panobinostat, and Methylstat. Lysates were cleared by centrifugation at 13,000 rpm for 15 min at 4 °C. The resulting supernatants were subjected to immunoprecipitation using the indicated antibodies. Proteins were separated on 10–15 % SDS/PAGE gels and transferred onto PVDF membranes (Millipore, Billerica, MA, USA). Following blocking, membranes were incubated with specific primary antibodies at appropriate dilutions. This was followed by incubation with HRP-conjugated secondary antibodies and visualization using the ECL system (Bio-Rad).

3.14. Immunohistochemical (IHC) staining

The tissue underwent fixation in 4 % paraformaldehyde, followed by paraffin embedding and slicing into 5 μm sections. Following dewaxing, antigen repair was performed by boiling the sections in Tris/EDTA buffer (pH 9.0) for 5 min. A 30-min incubation with 3 % H2O2 blocked peroxidase, and subsequent blocking with 10 % goat serum for 1 h was carried out. The tissue sections were then exposed to the specific FDX1 antibody (12592-1-AP, 1:500, Proteintech) at 4 °C overnight. Following PBS washing, slides were incubated with a biotin-conjugated secondary antibody for 45 min, followed by washing. Immunohistochemical staining and DAB visualization were performed using the GTVision III detection system (Gene Tech, China). Finally, the slides were stained with hematoxylin and dehydrated.

3.15. Statistical analysis

R (version 4.0.5) and GraphPad Prism (version 6.0.1) were employed for all statistical analyses. Each experiment was conducted independently at least twice. Comparisons were carried out using a two-tailed paired Student's t-test, one-way ANOVA, or two-way ANOVA, as specified in the individual figures. Statistical significance was set at p < 0.05, considering it as statistically significant (*p < 0.05, **p < 0.01, ***p < 0.001, and ****p < 0.0001).
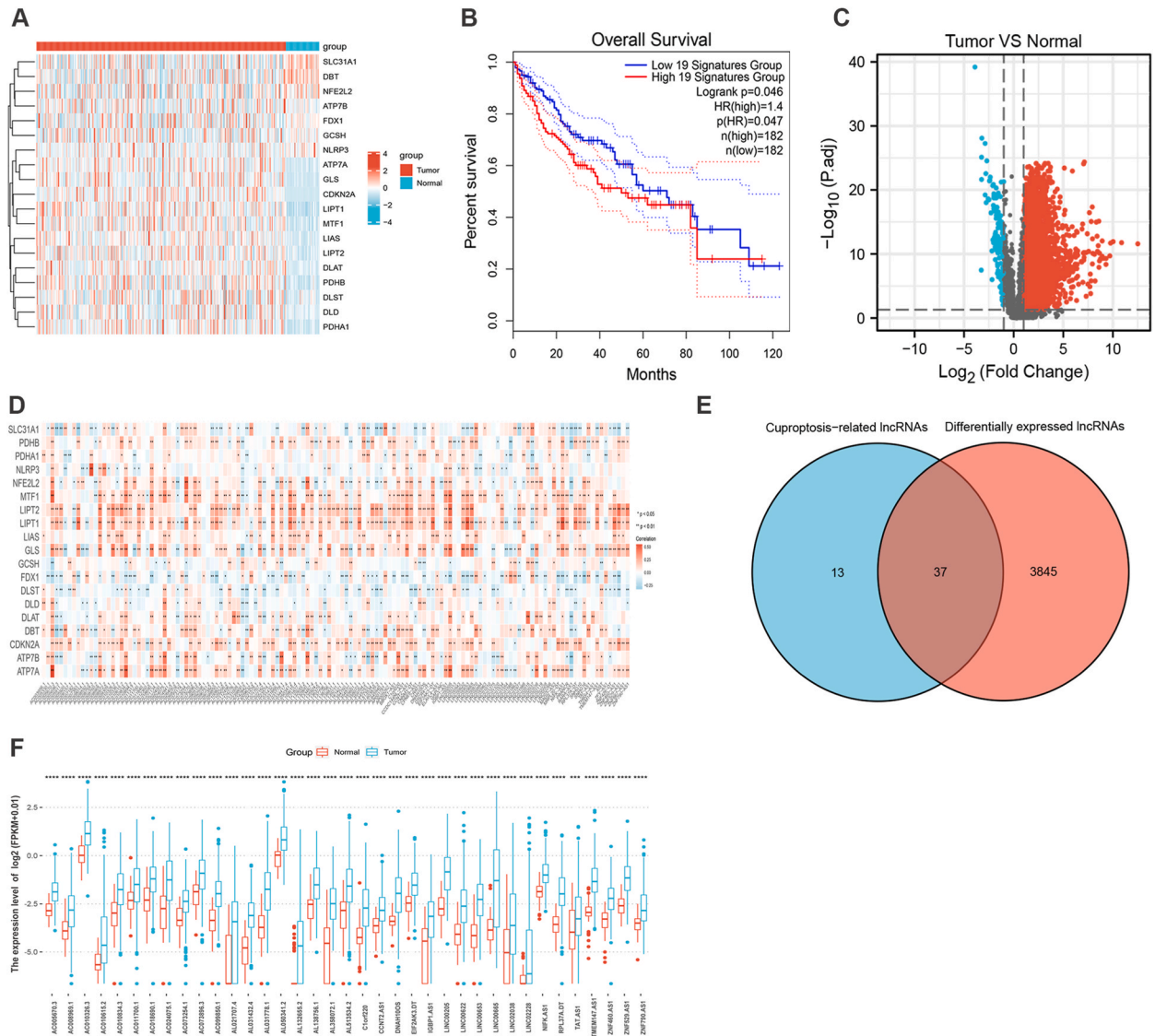
Fig. 1. Identification of cuproptosis-related lncRNAs (CRLs) in HCC. A. Expression levels of cuproptosis-related genes (CRGs) in normal liver tissue and HCC tumor tissue. B. Kaplan–Meier survival curves of overall survival of HCC patients between high and low expression groups of CRGs. C. The volcano plot of the differential expressed lncRNAs between the normal liver tissue samples and HCC samples. The screening criteria utilized were |log2 (Fold Change)| > 1 and adjusted p-value <0.01. The Benjamini–Hochberg (BH) method was employed for p-value correction. D. The correlation between differential expressed lncRNAs and CRGs in the TCGA dataset (method: Pearson's correlation analysis). Each unit's color indicated the degree of correlation. Red implied the positive relationship; blue was on the contrary. E. The overlap of differentially expressed lncRNAs and CRLs in HCC. F. Comparison of CRLs expression levels between normal liver tissue samples and HCC samples in the TCGA dataset. ns p > 0.05; *p < 0.05, **p < 0.01, ***p < 0.001, and ****p < 0.0001.

4. Results

### 4.1. Identification of CRLs in HCC

It is now widely recognized that lncRNAs serve as indicators of unique cell states or biological processes, potentially representing cellular pathologies such as cancer and serving as targets for therapeutic intervention [22,23]. However, research on lncRNAs associated with cuproptosis is limited. In this study, we investigated whether lncRNAs play a role in the response of HCC cells to copper.

Despite this, the occurrence of cuproptosis in various cancer types remains unclear. To address this gap, we examined the expression of CRGs. Our analysis unveiled significant differences in CRG expression levels between normal and HCC samples (Fig. 1A). To maintain intracellular copper homeostasis, ATP7A functions as a copper exporter [24], while SLC31A1 imports copper from the extracellular matrix into the cells [25]. In HCC, the expression of ATP7A was 1.5 times higher than that in normal tissues, whereas the expression of SLC31A1 was slightly lower. As illustrated in Fig. 1B, CRGs were found to negatively impact the prognosis of patients with HCC. Consequently, it is reasonable to posit that HCC cells exhibit resistance to the toxic effects of copper.

Subsequently, we conducted a differential expression analysis to identify aberrantly expressed HCC-lncRNAs (Fig. 1C). Our investigation pinpointed 50 lncRNAs that may be closely associated with cuproptosis in HCC (Fig. 1D). Among these, 37 CRLs exhibited high expression levels in tumor samples (Fig. 1E–F). In summary, our findings strongly link cuproptosis to the development and progression of HCC, and the identified 37 CRLs may play a pivotal role in regulating this process.

4.2. Construction of HCC risk model based on CRLs

To establish a robust risk model, patients with HCC were initially randomly assigned to two groups: a training group and a test group. Importantly, there were no discernible differences in clinical characteristics between these groups, as outlined in
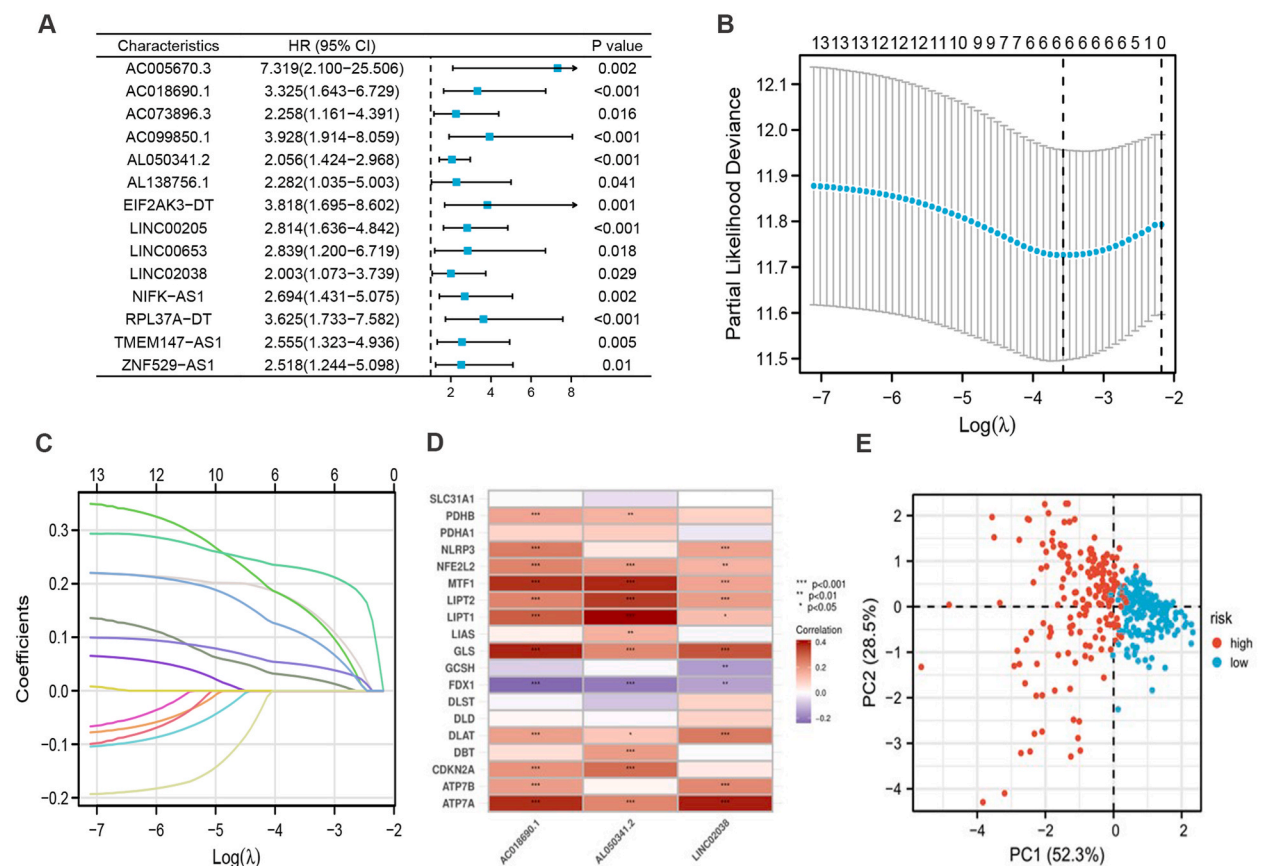
Fig. 2. Construction of HCC risk model based on CRLs. A. Univariate Cox regression of CRLs in HCC patients (threshold value: p-value< 0.05). B. Distribution of the LASSO coefficients of CRLs. C. The 10-fold cross-validation of variable selection in the LASSO algorithm. D. The correlation between 3 candidate CRLs and CRGs in the TCGA dataset (method: Pearson's correlation analysis). Each unit's color indicated the degree of correlation. Red implied the positive relationship, blue was on the contrary. E. PCA analysis confirmed a prominent difference between high- and low-risk groups.

ns p > 0.05; *p < 0.05, **p < 0.01, ***p < 0.001, and ****p < 0.0001.
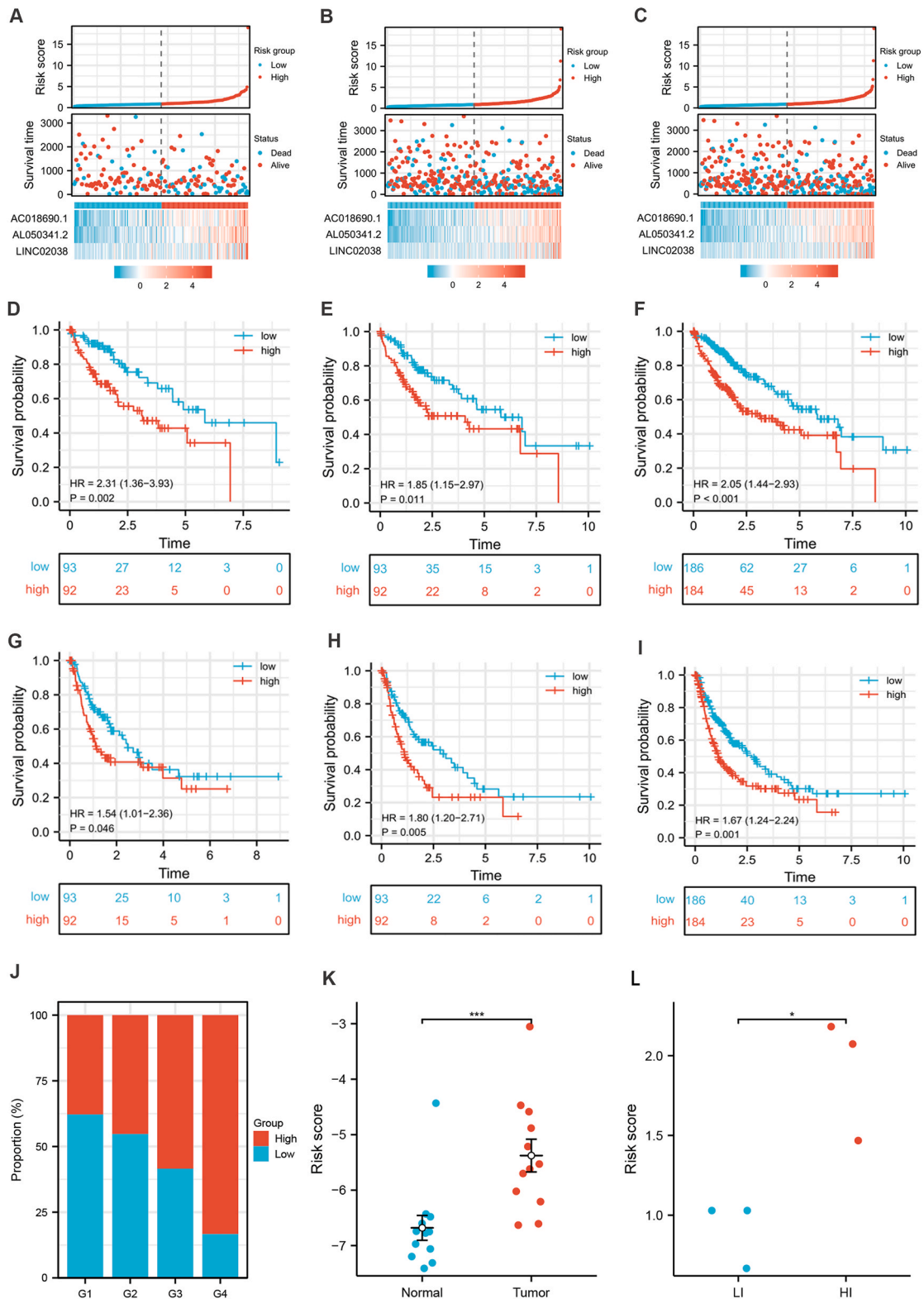
Fig. 3. Validation and improvement of the HCC risk model. A-C. The distribution of overall survival (OS) risk scores, survival time and survival status, heat maps of 3 CRLs expressions between high- and low-risk groups in the training (A), test (B), and TCGA groups (C), respectively. D-F. Kaplan–Meier survival curves of OS of HCC patients between high- and low-risk groups in the training (D), test (E), and TCGA groups (F), respectively. G-I. Kaplan–Meier survival curves of disease-free survival (DFS) of HCC patients between high- and low-risk groups in the training (G),

test (H), and TCGA groups (I), respectively. J. Distribution of patients with high- and low-risk in different grades of HCC. K. Comparison of risk scores between HCC samples and normal liver tissue samples in validation dataset (GSE115018). L. Comparison of risk scores between high-invasive (HI) and low-invasive (LI) HCC samples in validation dataset (clinical HCC samples).
ns p > 0.05; *p < 0.05, **p < 0.01, ***p < 0.001, and ****p < 0.0001.

◀━━━━━━

Supplementary Table 1. This random assignment strategy ensured a representative sample for the development of our risk model. The identification of critical CRLs involved a multi-step process. Firstly, a comprehensive univariate Cox analysis was conducted, focusing on fourteen lncRNAs that had the potential to influence the prognosis of patients with HCC (Fig. 2A). Subsequently, a LASSO regression analysis was applied to narrow down the selection to six lncRNAs, effectively addressing the issue of multicollinearity among variables (Fig. 2B–C). The final refinement of the CRLs involved a multivariate Cox analysis, which isolated three independent variables with a significant impact on patient prognosis. These variables—AC018690.1, AL050341.2, and LINC02038—were then used to construct the risk model, represented by the equation: risk score = 0.82 * *AC018690.1* + s0.65 * *AL050341.2* + 0.61 * *LINC02038*. We also examined the connections between these three CRLs and CRGs. As anticipated, we validated that all three were inversely correlated with FDX1, a pivotal regulator of protein lipoylation crucial in cuproptosis [15], and positively correlated with ATP7A and ATP7B, both copper exporters [26] (Fig. 2D).

Using the median risk score, we stratified patients with HCC into high- and low-risk groups. Principal component analysis (PCA) results indicated a significant distinction between these groups (Fig. 2E), confirming the robustness of the risk model based on CRLs.

### 4.3. Validation and improvement of the HCC risk model

We observed a consistent trend across the training (Fig. 3A, D, and 3G), test (Fig. 3B, E, and 3H), and TCGA groups (Fig. 3C, F, and 3I), where patients with lower risk scores exhibited better prognosis. In the overall survival (OS) analysis, hazard ratios were 2.31, 1.85, and 2.05 in the training, test, and TCGA groups, respectively (Fig. 3D–F). Additionally, the correlation between risk scores and disease-free survival (DFS) was evident, with hazard ratios of 1.54, 1.80, and 1.67, respectively (Fig. 3G–I). Furthermore, a positive correlation was identified between tumor grade and the proportion of high-risk patients (Fig. 3J). When comparing HCC to normal liver tissue samples (Fig. 3K) and high-invasive (HI) to low-invasive (LI) HCC samples (Fig. 3L), the observed significant increase in risk scores indicated a robust association between CRLs and HCC development and progression.

To improve the accuracy of the risk model, we conducted univariate and multivariate Cox analyses on the clinical information of patients with HCC. The results revealed that the clinical stage of patients could independently affect their prognosis (Supplementary Table 2). Consequently, we integrated this factor into the risk model to construct a nomogram (Fig. 4A). As anticipated, the calibration curve demonstrated excellent alignment of our proposed nomogram for survival prediction (Fig. 4B). This improved risk model more effectively and accurately reflected the patient survival status (Fig. 4C).

4.4. Correlation between HCC risk model and tumor immune microenvironment (TIME) of patients with HCC

The diversity of immune cells within the tumor immune microenvironment (TIME) plays a pivotal role in cancer progression [27]. Consequently, our interest was piqued regarding potential disparities in TIME between high- and low-risk groups. Initially, we assessed immune cell components through ssGSEA based on key markers of 23 immune cells [19]. Our findings indicated that over 60 % of common immune cells exhibited significant differences in tumor-infiltrating levels between the high- and low-risk groups (Fig. 5A).

A noteworthy observation was the positive correlation between the number of T helper 2 (Th2) cells and risk scores (Fig. 5B). Given that Th2 cells counteract the antitumor effect of T helper 1 (Th1) cells [28]. Simultaneously, we confirmed an inverse correlation
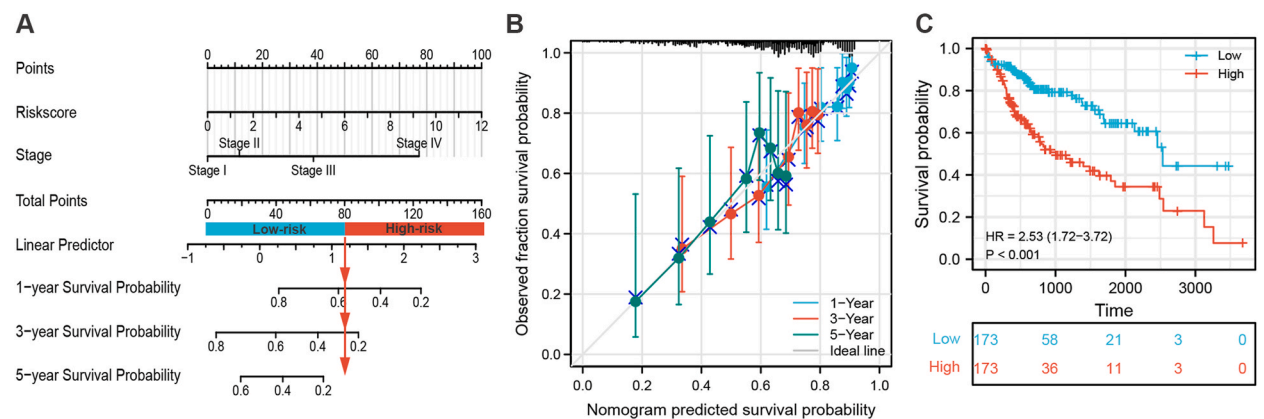
Fig. 4. Construction and validation of an optimized nomogram based on CRLs. A. A nomogram combining clinical stage and risk scores predicts 1-, 3-, and 5-years overall survival in patients with HCC. B. Calibration curves test the agreement between actual and predicted outcomes at 1, 3, and 5 years. C. Kaplan–Meier survival curves of OS of HCC patients between high- and low-risk groups after optimization.
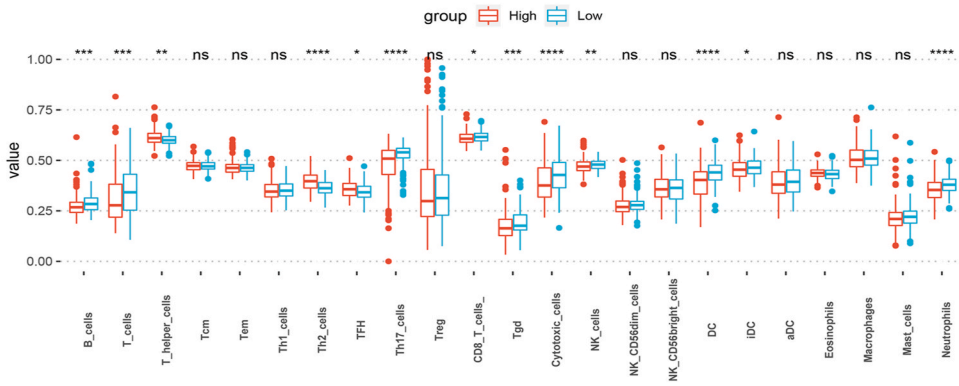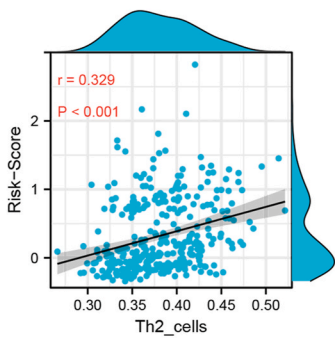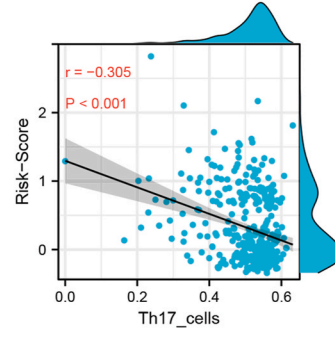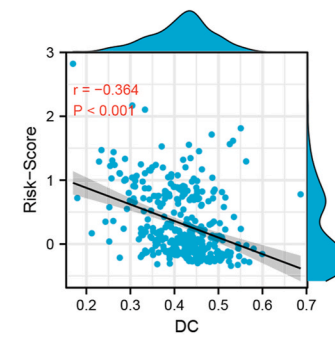
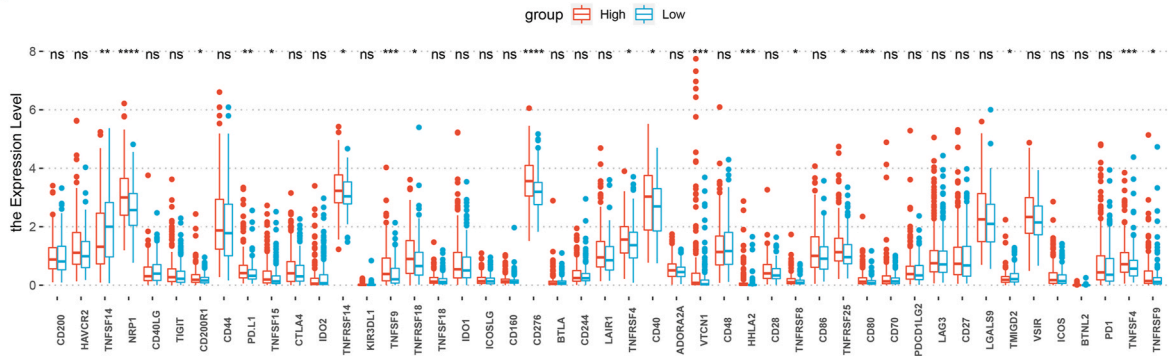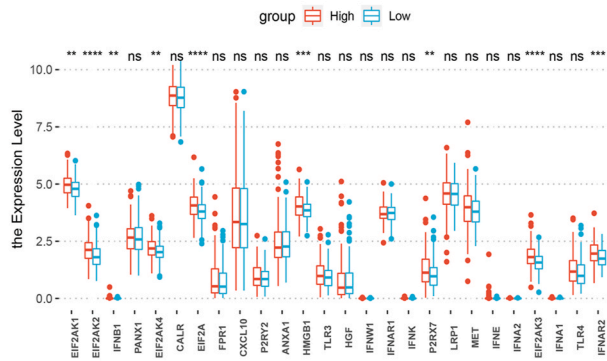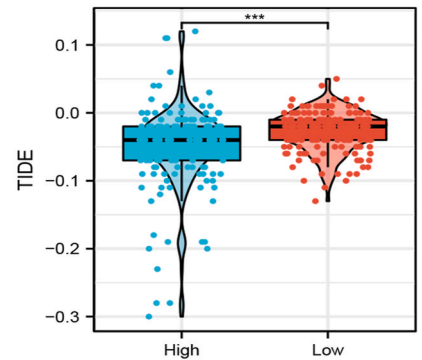(caption on next page)

Fig. 5. The correlation between HCC risk model and TIME of HCC patients. A. Differential enrichment scores of 23 immune cell types among HCC risk groups in TCGA. B-D. Correlation between optimized risk model scores and the contents of T helper 2 cells (B), T helper cells 17 (C) and Dendritic Cells (D). E-F. Differential expression of ICPs (E) and ICD-related genes (F) among the high- and low-risk groups in TCGA. **G.** Comparison of TIDE prediction score between the high- and low-risk groups.
ns $p > 0.05$; *$p < 0.05$, **$p < 0.01$, ***$p < 0.001$, and ****$p < 0.0001$.

---

between the infiltration of Th17 cells (directly activating CD8^{+} T cells) and dendritic cells (DCs, activating T cells to trigger an antitumor response) and risk scores [29,30] (Fig. 5C–D).

The landscape of cancer treatment has been profoundly impacted by remarkable advancements in immune checkpoint (ICP) blockade therapies [30,31]. Intriguingly, PD-L1 and more than ten types of ICPs exhibited significant differences in expression between the high- and low-risk groups (Fig. 5E). Additionally, it is crucial to note that cancer cells have developed intricate mechanisms to evade the recognition of cell death as immunogenic [32]. As illustrated in Fig. 5F, the genes associated with immunogenic cell death (ICD) varied between the constructed models.

The Tumor Immune Dysfunction and Exclusion (TIDE) prediction score serves as an indicator of the potential for immune evasion and dysfunction within a tumor [19,20]. Based on the lower TIDE scores observed among patients in the high-risk group, it can be inferred that their likelihood of experiencing immune escape was comparatively reduced. Consequently, these individuals might have a higher probability of deriving therapeutic advantages from immunotherapeutic interventions (Fig. 5G).

In summary, the risk model constructed using CRLs has the potential to reflect the TIME of patients and provide valuable insights for the immunotherapy of HCC.

4.5. Clinical characteristics, treatment prediction and molecular analysis of risk groups

The pathological grade of a tumor holds significant importance in determining its malignancy level [33]. Grade III samples, primarily from high-risk group patients, affirm the validity of our risk model (Fig. 6A). ADH1A and PYCR2 play roles in the metabolic reprogramming of HCC and stand out as novel prognostic biomarkers [34]. In the high-risk group, the expression of ADH1A—associated with favorable patient outcomes—was notably lower. Additionally, the high-risk group exhibited lower expression of PYCR2, a gene linked to shorter survival (Fig. 6B–C). Moreover, the mutation rate in the high-risk group slightly surpassed that in the low-risk group (Fig. 6D–E). The intriguing observation of a significant decrease in TP53 mutation frequency from the high-risk to the low-risk group prompts further exploration. Multiple studies indicate that mutant p53 stimulates glycolysis, suppresses oxidative phosphorylation, and modulates lipid metabolism, potentially enhancing cancer cell evasion through these mechanisms [35]. However, additional studies are necessary for a comprehensive understanding of these mechanisms.

Sorafenib, targeting VEGF receptor, RAF, and PDGF receptor, has demonstrated a substantial extension of OS in patients with advanced HCC [36], while Dasatinib can induce cell cycle arrest and apoptosis in "progenitor" HCC cell lines [37]. Through a predictive analysis of drug sensitivity, we showcased that high-risk patients exhibited significantly reduced sensitivity to these drugs (Fig. 6F–G).

To delve into the potential mechanisms affecting sensitivity to copper toxicity, we conducted an analysis of relevant pathways using gene ontology (GO) and Kyoto Encyclopedia of Genes and Genomes (KEGG) based on differentially expressed genes between the high- and low-risk groups (Fig. 6H–J). The results indicate the involvement of DNA replication origin binding, cell cycle, and ECM-receptor interactions in this process.
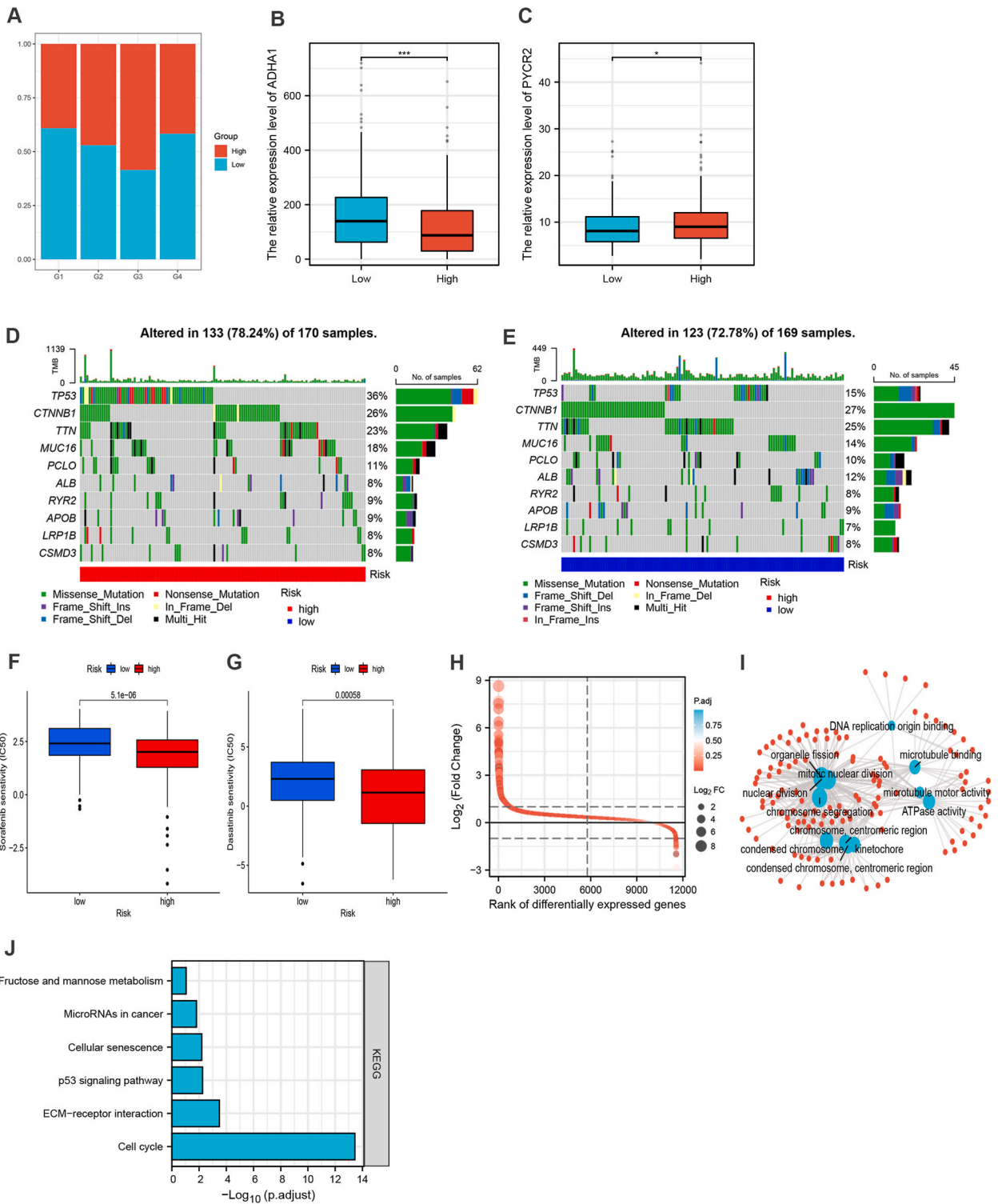
In summary, the high- and low-risk groups exhibited marked differences in clinical, therapeutic, and molecular aspects, suggesting that CRLs may serve as essential regulators of HCC.

4.6. In vitro validation of the association between lncRNAs and cuptoptosis

To provide substantive and compelling evidence for the CRLs in our model, we treated HCC cells (Huh7 and HCCLM3) with Elesclomol (100 nM)-Cu (100μM) and assessed the resulting cell death rate induced by copper overload. Remarkably, our findings revealed that both Huh7 and HCCLM3 cells exhibited significant resistance to cuproptosis (cell death rate <20 %). However, upon silencing AC018690.1, AL050341.2, and LINC02038, we observed a marked increase in cytotoxicity caused by copper overload (Fig. 7A–C).

Cuproptosis arises from the direct binding of copper to the lipoacylated components of the TCA cycle, leading to the aggregation of lipoacylated proteins and, ultimately, proteotoxic stress and cell death. Thus, heightened lipoacylation serves as a hallmark event in cuproptosis [14]. As anticipated, immunoblotting results demonstrated that silencing AC018690.1, AL050341.2, and LINC02038 significantly intensified intracellular lipoacylation (Fig. 7D), firmly establishing the link between CRL candidates and cuproptosis. Furthermore, high-risk HCC samples, indicative of a substantial invasion propensity, exhibited a noticeable reduction in the expression levels of FDX1 (Fig. 7E–F).

Consequently, targeting these lncRNAs has the potential to enhance the efficacy of copper ionophores against HCC, thereby fostering the development of novel therapies that build upon existing modalities (such as first-line drugs, immunotherapy and copper ionophores).

A

B The relative expression level of ADHA1

C The relative expression level of PYCR2

D Altered in 133 (78.24%) of 170 samples.

E Altered in 123 (72.78%) of 169 samples.

F Sorafenib sensitivity (IC50)

G Dasatinib sensitivity (IC50)

H

I

J

(caption on next page)

Fig. 6. Clinical characteristics, treatment prediction and molecular analysis of high/low risk groups. A. Distribution of patients with high- and low-risk (the optimized risk model) in different grades of HCC. B. Comparison of ADH1A expression levels among risk groups in the TCGA dataset. C. Comparison of PYCR2 expression levels among risk groups in the TCGA dataset. D-**E.** Waterfall plot of top 10 mutant genes in the high- (D) and low-risk group (E) in HCC.

F-G. Box plot of drug sensitivity to Sorafenib (F) and Dasatinib (G) in high- and low-risk groups

H. Differential gene expression in high- and low-risk groups of HCC.

I-J. Gene Ontology (GO) (H) and Kyoto Encyclopedia of Genes and Genomes (KEGG) (I) pathway enrichment analysis. The BH method was applied for p-value correction, with a threshold set at p-value <0.05.

ns $p > 0.05$; *$p < 0.05$, **$p < 0.01$, ***$p < 0.001$, and ****$p < 0.0001$.

5. Discussion

Encouragingly, Tsvetkov et al. proposed a unique form of regulated cell death- "cuproptosis" [15]. While copper chelation therapy has demonstrated its efficacy for treating copper metabolic diseases, such as Wilson's disease [12], the utilization of copper ionophores in cancer treatment remains limited in terms of effectiveness [31].

Recent genome-wide representation of the human cancer transcriptome has demonstrated that lncRNA expression is one of the most prevalent transcriptional changes in cancer [32]. Some lncRNAs mediate tumourigenesis or tumour suppression and are potential targets for cancer treatment. However, only a few lncRNAs have been functionally characterized [33]. There is limited evidence linking lncRNAs to coproptosis. Therefore, our study aimed to explore lncRNA targets closely related to copper toxicity to improve the effect of copper ionophores in cancer treatment and provide a theoretical basis for the comprehensive treatment of HCC.

First, 37 lncRNAs closely related to cuproptosis and abnormally expressed in HCC were identified. Among these, we determined that AC018690.1, AL050341.2, and LINC02038 were closely related to patient prognosis using univariate Cox analysis, LASSO regression analysis, and multivariate Cox analysis. Considering the importance of clinical diagnosis, we added clinical stage (which could affect the prognosis of patients as an independent factor) into our model, which improved the accuracy and validity of the risk model and was more conducive to prospectively predicting patient survival. This has a guiding significance for clinical decision-making.

To determine the potential mechanisms by which candidate CRLs affect resistance to copper toxicity, we analyzed the cellular, functional, and molecular characteristics of the high- and low-risk groups. On the one hand, the contents of 13 kinds of immune cells differ in two groups, in which Th2 cells, Th17 cells and DCs were strongly correlated with risk scores in our model. Hence, it is reasonable to believe that the TIME is also involved in the association between lncRNA targets and cuproptosis, which is also explained by the differences between ICPs and ICD-related genes.

The differences in pathological grade and tumour biomarker expression also proved the feasibility of our model from another perspective. Functional enrichment analysis revealed that the differences between the two groups mainly existed in the cell cycle, ECM-receptor receptor, and p53 signalling pathways. Cell cycle abnormalities are important features of cancer [34], while extra-cellular matrix (ECM) components have been identified as important modulators of cancer progression [35]. Additionally, p53 mutations occur frequently in human HCC [36]. The observed variations in the frequency of p53 mutations between the high- and low-risk groups indicate that there may be a regulatory role for CRLs in the cuproptosis process in HCC via these pathways.

Notably, our study provided unique insights into the treatment of HCC based on cuproptosis. First, the TIDE scores showed that patients in the high-risk group were more likely to benefit from immunotherapy. Therefore, immunotherapy can be applied to patients with HCC with high expression of AC018690.1, AL050341.2, and LINC02038. In addition, high-risk patients show poor sensitivity to sorafenib and dasatinib, and targeting lncRNAs may improve drug efficacy. Furthermore, experiments *in vitro* have verified that these targets significantly affect the death of HCC cells caused by copper ionophores. In this study, we constructed a risk model with clinical practicability and proposed a new comprehensive treatment scheme for HCC based on the regulation of cuproptosis by lncRNA targets, thus opening a new horizon for HCC treatment.

However, this study had several limitations. Owing to the lack of sequencing and clinical follow-up data from sufficient HCC samples, this risk model has not yet been shown to be applicable to all HCC subtypes for defining cuproptosis-based therapy regimens. Our *in vitro* experiments were dependent on HCC cell lines and may not completely reflect the intricate nature of tumors. The molecular processes underlying the regulation of cuproptosis by these three HCC CRLs remain unknown. Therefore, an extensive experimental investigation is necessary.

6. Conclusions

Among the lncRNAs associated with cuproptosis and abnormally expressed in HCC, we identified AC018690.1, AL050341.2, and LINC02038 as clearly associated with the prognosis of patients with HCC. Furthermore, we developed an innovative risk model based on targets and key clinical factors, and patients with HCC were divided into high- and low-risk groups based on their risk scores. Our analysis found significant differences in TIME, molecular and clinical characteristics between the risk groups. The remarkable effect of the CRLs targets on Cu toxicity resistance was verified *in vitro*. In conclusion, our study constructed a risk model which could not only predict the survival of patients with HCC but also provide comprehensive and meaningful HCC treatment.
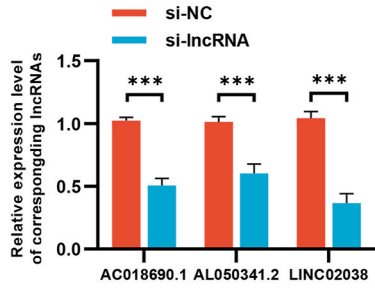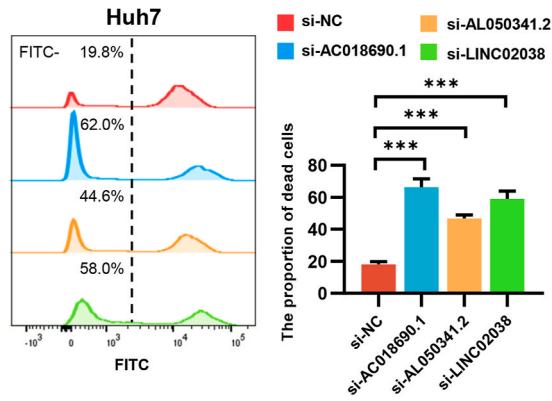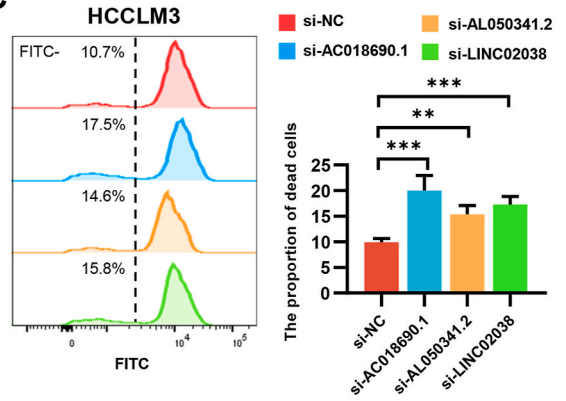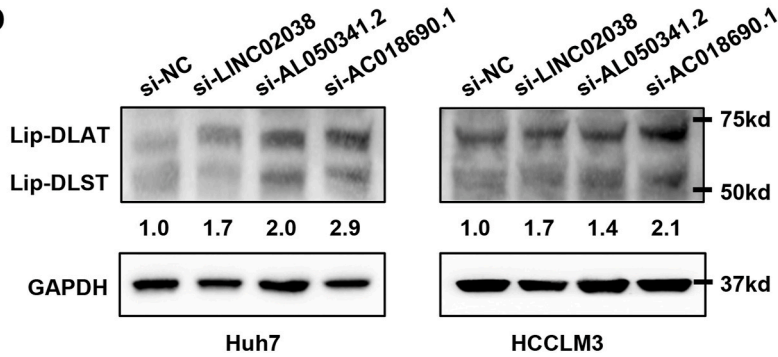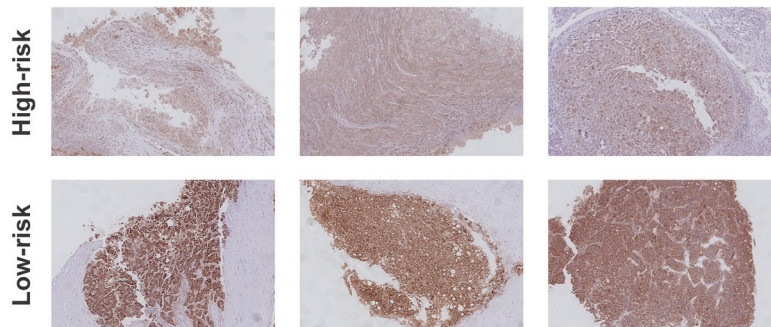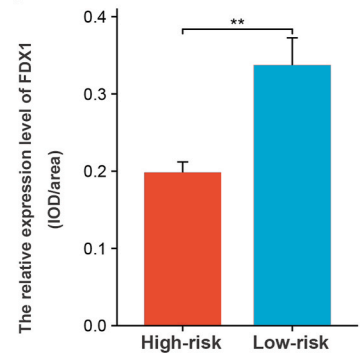
(caption on next page)

Fig. 7. *In vitro* validation of the association between lncRNAs and cuptoptosis. **A.** RT-qPCR were used to verify the knock-down efficiency of siRNAs against specific lncRNAs.

B–C. Left: Flow cytometry results showed the proportion of dead cells ($CFSE^-$) in si-NC, si-AC018690.1, si-AL050341.2 and si-LINC02038 groups (B for Huh7 cells, and C for HCCLM3 cells) after 2 h s shock with Elesclomol (100 nM) -Cu (100μM). Right: the proportion of dead cells of different groups are quantified (B for Huh7 cells, and C for HCCLM3 cells)

D. Huh7 and HCCLM3 cells in si-NC, si-AC018690.1, si-AL050341.2 and si-LINC02038 groups were treated with Elesclomol (200 nM)- Cu (1 M) shock for 2 h s. After 24 h s, the degree of lipoacylation was analyzed by immunoblotting and the antibody described in the description. GAPDH was used as an internal reference

E. Comparison of protein expression patterns of FDX1 in clinical HCC samples between the high- and low-risk group using Immunohistochemistry (IHC) assays (20 ×)

F. The expression levels of FDX1 among risk groups were compared by immunohistochemistry. IOD/area denotes the mean optical density of the areas of interest

ns $p > 0.05$; *$p < 0.05$, **$p < 0.01$, ***$p < 0.001$, and ****$p < 0.0001$.

Consent for publication

The authors have no conflicts of interest to declare.

Data availability statement

Data associated with this study has been deposited at The Cancer Genome Atlas (TCGA, https://portal.gdc.cancer.gov/) database and the NCBI GEO database (http://www.ncbi.nlm.nih.gov/geo/, record number GSE115018). And the data of clinical samples will be made available upon request.

Ethics statement

The authors declare that they have no known competing financial interests or personal relationships that could have appeared to influence the work reported in this paper.

CRediT authorship contribution statement

Jing He: Writing – original draft, Visualization, Methodology, Investigation. **Weiqi Li:** Writing – original draft, Validation, Methodology. **Weijun Zhao:** Validation. **Hao Shen:** Validation, Supervision. **Yushun Chang:** Writing – review & editing, Validation. **Boqiang Liu:** Visualization, Funding acquisition, Data curation. **Qiang He:** Writing – review & editing, Supervision. **Hong Yu:** Writing – review & editing, Funding acquisition. **Yifan Wang:** Writing – review & editing, Supervision. **Liang Shi:** Funding acquisition, Data curation. **Xiujun Cai:** Project administration, Funding acquisition, Formal analysis.

Declaration of competing interest

The authors declare that they have no known competing financial interests or personal relationships that could have appeared to influence the work reported in this paper.

Appendix A. Supplementary data

Supplementary data to this article can be found online at https://doi.org/10.1016/j.heliyon.2024.e24453.

References

[1] L. Wei, D. Lee, C.T. Law, M.S. Zhang, J. Shen, D.W. Chin, C.M. Wong, Genome-wide CRISPR/Cas9 library screening identified PHGDH as a critical driver for Sorafenib resistance in HCC, Nat. Commun. 10 (1) (2019) 4681, https://doi.org/10.1038/s41467-019-12606-7.

[2] Y. Shimizu, N. Peltzer, A. Sevko, E. Lafont, A. Sarr, H. Draberova, H. Walczak, The Linear ubiquitin chain assembly complex acts as a liver tumor suppressor and inhibits hepatocyte apoptosis and hepatitis, Hepatology 65 (6) (2017) 1963–1978, https://doi.org/10.1002/hep.29074.

[3] T.Y. Lee, Y.C. Hsu, H.C. Tseng, S.H. Yu, J.T. Lin, M.S. Wu, C.Y. Wu, Association of Daily Aspirin therapy with risk of hepatocellular carcinoma in patients with chronic hepatitis B, JAMA Intern. Med. 179 (5) (2019) 633–640, https://doi.org/10.1001/jamainternmed.2018.8342.

[4] J.S.V. Lally, S. Ghoshal, D.K. DePeralta, O. Moaven, L. Wei, R. Masia, B.C. Fuchs, Inhibition of acetyl-CoA carboxylase by phosphorylation or the inhibitor ND-654 suppresses lipogenesis and hepatocellular carcinoma, Cell Metabol. 29 (1) (2019) 174–182, https://doi.org/10.1016/j.cmet.2018.08.020, e175.

[5] J.M. Mato, M.L. Martinez-Chantar, S.C. Lu, Systems biology for hepatologists, Hepatology 60 (2) (2014) 736–743, https://doi.org/10.1002/hep.27023.

[6] W. Gao, Z. Tang, Y.F. Zhang, M. Feng, M. Qian, D.S. Dimitrov, M. Ho, Immunotoxin targeting glypican-3 regresses liver cancer via dual inhibition of Wnt signalling and protein synthesis, Nat. Commun. 6 (2015) 6536, https://doi.org/10.1038/ncomms7536.

[7] Q. Xu, Y. Li, X. Gao, K. Kang, J.G. Williams, L. Tong, X. Li, HNF4alpha regulates sulfur amino acid metabolism and confers sensitivity to methionine restriction in liver cancer, Nat. Commun. 11 (1) (2020) 3978, https://doi.org/10.1038/s41467-020-17818-w.

[8] B.E. Kim, T. Nevitt, D.J. Thiele, Mechanisms for copper acquisition, distribution and regulation, Nat. Chem. Biol. 4 (3) (2008) 176–185, https://doi.org/10.1038/nchembio.72.

[9] L. Cui, A.M. Gouw, E.L. LaGory, S. Guo, N. Attarwala, Y. Tang, J. Rao, Mitochondrial copper depletion suppresses triple-negative breast cancer in mice, Nat. Biotechnol. 39 (3) (2021) 357–367, https://doi.org/10.1038/s41587-020-0707-9.

[10] J.R. Prohaska, A.A. Gybina, Intracellular copper transport in mammals, J. Nutr. 134 (5) (2004) 1003–1006, https://doi.org/10.1093/jn/134.5.1003.

[11] F. Ren, B.L. Logeman, X. Zhang, Y. Liu, D.J. Thiele, P. Yuan, X-ray structures of the high-affinity copper transporter Ctr1, Nat. Commun. 10 (1) (2019) 1386, https://doi.org/10.1038/s41467-019-09376-7.

[12] J.P. Hamilton, L. Koganti, A. Muchenditsi, V.S. Pendyala, D. Huso, J. Hankin, S. Lutsenko, Activation of liver X receptor/retinoid X receptor pathway ameliorates liver disease in Atp7B(-/-) (Wilson disease) mice, Hepatology 63 (6) (2016) 1828–1841, https://doi.org/10.1002/hep.28406.

[13] M. Yang, X. Wu, J. Hu, Y. Wang, Y. Wang, L. Zhang, J. Guan, COMMD10 inhibits HIF1alpha/CP loop to enhance ferroptosis and radiosensitivity by disrupting Cu-Fe balance in hepatocellular carcinoma, J. Hepatol. 76 (5) (2022) 1138–1150, https://doi.org/10.1016/j.jhep.2022.01.009.

[14] Q. Xue, R. Kang, D.J. Klionsky, D. Tang, J. Liu, X. Chen, Copper metabolism in cell death and autophagy, Autophagy 19 (8) (2023) 2175–2195, https://doi.org/10.1080/15548627.2023.2200554.

[15] P. Tsvetkov, S. Coy, B. Petrova, M. Dreishpoon, A. Verma, M. Abdusamad, T.R. Golub, Copper induces cell death by targeting lipoylated TCA cycle proteins, Science 375 (6586) (2022) 1254–1261, https://doi.org/10.1126/science.abf0529.

[16] Y. Hosono, Y.S. Niknafs, J.R. Prensner, M.K. Iyer, S.M. Dhanasekaran, R. Mehra, A.M. Chinnaiyan, Oncogenic role of THOR, a conserved cancer/testis long non-coding RNA, Cell 171 (7) (2017) 1559–1572, https://doi.org/10.1016/j.cell.2017.11.040, e1520.

[17] P. Carotenuto, M. Fassan, R. Pandolfo, A. Lampis, C. Vicentini, L. Cascione, C. Braconi, Wnt signalling modulates transcribed-ultraconserved regions in hepatobiliary cancers, Gut 66 (7) (2017) 1268–1277, https://doi.org/10.1136/gutjnl-2016-312278.

[18] M.K. Iyer, Y.S. Niknafs, R. Malik, U. Singhal, A. Sahu, Y. Hosono, A.M. Chinnaiyan, The landscape of long noncoding RNAs in the human transcriptome, Nat. Genet. 47 (3) (2015) 199–208, https://doi.org/10.1038/ng.3192.

[19] G. Bindea, B. Mlecnik, M. Tosolini, A. Kirilovsky, M. Waldner, A.C. Obenauf, J. Galon, Spatiotemporal dynamics of intratumoral immune cells reveal the immune landscape in human cancer, Immunity 39 (4) (2013) 782–795, https://doi.org/10.1016/j.immuni.2013.10.003.

[20] J. Fu, K. Li, W. Zhang, C. Wan, J. Zhang, P. Jiang, X.S. Liu, Large-scale public data reuse to model immunotherapy response and resistance, Genome Med. 12 (1) (2020) 21, https://doi.org/10.1186/s13073-020-0721-z.

[21] P. Jiang, S. Gu, D. Pan, J. Fu, A. Sahu, X. Hu, X.S. Liu, Signatures of T cell dysfunction and exclusion predict cancer immunotherapy response, Nat. Med. 24 (10) (2018) 1550–1558, https://doi.org/10.1038/s41591-018-0136-1.

[22] A.M. Schmitt, H.Y. Chang, Long noncoding RNAs in cancer pathways, Cancer Cell 29 (4) (2016) 452–463, https://doi.org/10.1016/j.ccell.2016.03.010.

[23] C. Lin, L. Yang, Long noncoding RNA in cancer: wiring signaling circuitry, Trends Cell Biol. 28 (4) (2018) 287–301, https://doi.org/10.1016/j.tcb.2017.11.008.

[24] L.M. Guthrie, S. Soma, S. Yuan, A. Silva, M. Zulkifli, T.C. Snavely, J.C. Sacchettini, Elesclomol alleviates Menkes pathology and mortality by escorting Cu to cuproenzymes in mice, Science 368 (6491) (2020) 620–625, https://doi.org/10.1126/science.aaz8899.

[25] T.A. Su, D.S. Shihadih, W. Cao, T.C. Detomasi, M.C. Heffern, S. Jia, C.J. Chang, A modular ionophore platform for liver-directed copper supplementation in cells and animals, J. Am. Chem. Soc. 140 (42) (2018) 13764–13774, https://doi.org/10.1021/jacs.8b08014.

[26] T. Fang, W. Chen, Y. Sheng, S. Yuan, Q. Tang, G. Li, Y. Liu, Tetrathiomolybdate induces dimerization of the metal-binding domain of ATPase and inhibits platination of the protein, Nat. Commun. 10 (1) (2019) 186, https://doi.org/10.1038/s41467-018-08102-z.

[27] J.D. Butner, D. Elganainy, C.X. Wang, Z. Wang, S.H. Chen, N.F. Esnaola, V. Cristini, Mathematical prediction of clinical outcomes in advanced cancer patients treated with checkpoint inhibitor immunotherapy, Sci. Adv. 6 (18) (2020) eaay6298, https://doi.org/10.1126/sciadv.aay6298.

[28] T.R. Mosmann, H. Cherwinski, M.W. Bond, M.A. Giedlin, R.L. Coffman, Two types of murine helper T cell clone. I. Definition according to profiles of lymphokine activities and secreted proteins, J. Immunol. 136 (7) (1986) 2348–2357.

[29] N. Martin-Orozco, C. Dong, The IL-17/IL-23 axis of inflammation in cancer: friend or foe? Curr. Opin. Invest. Drugs 10 (6) (2009) 543–549.

[30] F. Zhao, C. Xiao, K.S. Evans, T. Theivanthiran, N. DeVito, A. Holtzhausen, B.A. Hanks, Paracrine wnt5a-beta-catenin signaling triggers a metabolic Program that drives dendritic cell tolerization, Immunity 48 (1) (2018) 147–160, https://doi.org/10.1016/j.immuni.2017.12.004, e147.

[31] S.J. O'Day, A.M. Eggermont, V. Chiarion-Sileni, R. Kefford, J.J. Grob, L. Mortier, A. Hauschild, Final results of phase III SYMMETRY study: randomized, double-blind trial of elesclomol plus paclitaxel versus paclitaxel alone as treatment for chemotherapy-naive patients with advanced melanoma, J. Clin. Oncol. 31 (9) (2013) 1211–1218, https://doi.org/10.1200/JCO.2012.44.5585.

[32] Z. Wang, B. Yang, M. Zhang, W. Guo, Z. Wu, Y. Wang, D. Yang, lncRNA epigenetic landscape analysis identifies EPIC1 as an oncogenic lncRNA that interacts with MYC and promotes cell-cycle progression in cancer, Cancer Cell 33 (4) (2018) 706–720, https://doi.org/10.1016/j.ccell.2018.03.006, e709.

[33] Z. Du, T. Sun, E. Hacisuleyman, T. Fei, X. Wang, M. Brown, Liu X.S. Integrative analyses reveal a long noncoding RNA-mediated sponge regulatory network in prostate cancer, Nat. Commun. 7 (2016) 10982, https://doi.org/10.1038/ncomms10982.

[34] T. Otto, P. Sicinski, Cell cycle proteins as promising targets in cancer therapy, Nat. Rev. Cancer 17 (2) (2017) 93–115, https://doi.org/10.1038/nrc.2016.138.

[35] C.L. Hedegaard, C. Redondo-Gomez, B.Y. Tan, K.W. Ng, D. Loessner, A. Mata, Peptide-protein coassembling matrices as a biomimetic 3D model of ovarian cancer, Sci. Adv. 6 (40) (2020), https://doi.org/10.1126/sciadv.abb3298.

[36] Y.D. Luo, L. Fang, H.Q. Yu, J. Zhang, X.T. Lin, X.Y. Liu, C.M. Xie, p53 haploinsufficiency and increased mTOR signalling define a subset of aggressive hepatocellular carcinoma, J. Hepatol. 74 (1) (2021) 96–108, https://doi.org/10.1016/j.jhep.2020.07.036.

[37] R.S. Finn, A. Aleshin, J. Dering, P. Yang, C. Ginther, A. Desai, D.J. Slamon, Molecular subtype and response to dasatinib, an Src/Abl small molecule kinase inhibitor, in hepatocellular carcinoma cell lines in vitro, Hepatology 57 (5) (2013) 1838–1846, https://doi.org/10.1002/hep.26223.